



Cite this: *J. Mater. Chem. C*, 2022, 10, 9538

Pure bromide-based inorganic perovskite sky-blue light-emitting diodes through phase control by the NiO_x anode interface†

Kai Sun,^{ab} Zhiqiang Bao,^{ab} Xiaoyang Guo,^{id}*^a Jianfeng Ou,^{ab} Ying Lv,^{id}^a Deyue Zou,^{ab} Li Song,^{id}*^c Yantao Li,^a Xingyuan Liu^a and Jingqiu Liang*^a

Perovskite light-emitting diodes (PeLEDs) have been considered as a potential technology for next-generation lighting and displays. However, the relatively primitive blue-emitting devices obtained have limited the development of PeLEDs. Therefore, there is an urgent need to develop new preparation methods and regulation strategies for blue PeLEDs. Herein, a simple and efficient strategy has been reported for blue PeLEDs based on pure bromide perovskites without any doping using a NiO_x anode interface. The effects of NiO_x on the composition and morphology of the perovskite films were analyzed in detail. NiO_x replaced PEDOT:PSS as the anode interface layer, which promoted the formation of Cs₄PbBr₆, thus effectively restricting the growth of CsPbBr₃ and widening the perovskite bandgap, achieving a blue PeLED. Eventually, a sky-blue PeLED with a maximum luminance of 1610 cd m⁻² and a maximum external quantum efficiency of 1.58% was achieved. Our work will provide a simple and feasible scheme for the development of efficient and stable blue PeLEDs based on pure bromide perovskites, as well as providing useful studies for the realization of blue PeLEDs through phase composition regulated by interface control.

Received 6th April 2022,
Accepted 23rd May 2022

DOI: 10.1039/d2tc01395a

rsc.li/materials-c

Introduction

Perovskite light-emitting diodes (PeLEDs) have the advantages of a high fluorescence quantum efficiency, a wide color gamut, easy processing, *etc.*, which present great potential applications for next-generation lighting and displays.^{1–3} During the past few years, considerable progress has been achieved for PeLEDs with external quantum efficiency (EQE) values exceeding 20% in green, red, and near-infrared devices.^{3–7} However, the performance of blue PeLEDs remains significantly behind other devices, with the highest EQE of 13.8% in the sky-blue region between 475 nm and 490 nm.^{8–10} Therefore, it is very important to develop new preparation methods and regulation strategies for blue PeLEDs with both high efficiency and high brightness.^{11–15}

Recently, remarkable progress has been made in low-dimensional or quantum-dot perovskite blue-light-emitting

devices with energy band regulation based on the quantum confinement effect. Among these studies, large-sized organic cations, such as ethylammonium (EA), phenylethylammonium (PEA), and butylammonium (BA), as well as long-chain organic ligands of oleylamine and oleic acid, have been introduced to tune the bandgap and crystallization morphology, and impressive progress has been achieved in developing efficient blue PeLEDs.^{16–23} However, these devices still suffer from the problems of decreased charge injection and lowered brightness from the reduced electrical conductivity due to the introduced organic components.^{24–28} In addition, modulating the halide anions is another commonly adopted way to widen the bandgap of perovskites for the realization of blue emission.^{11,29,30} However, the mixed-halide (Br/Cl) blue PeLEDs suffer from ion migration and phase segregation under the action of water vapor, oxygen, and electric fields, resulting in increased defect densities and poor colour stability.^{15,31} Therefore, it may be feasible to develop pure bromide-based PeLEDs instead of mixed-halide systems to realize blue-emitting PeLEDs.

It is well known that CsPbBr₃ is a pure bromide-based inorganic perovskite, which has been extensively investigated as a green-emissive material for PeLEDs. Cs₄PbBr₆ is another Cs–Pb–Br-based material, which can be formed by adjusting the Cs/Pb ratio.^{32,33} The Cs-rich phase Cs₄PbBr₆ possesses unique structural and optical properties. Compared with

^a State Key Laboratory of Luminescence and Applications, Changchun Institute of Optics, Fine Mechanics and Physics, Chinese Academy of Sciences, Changchun 130033, China. E-mail: guoxy@ciomp.ac.cn

^b University of Chinese Academy of Sciences, Beijing 100049, China

^c Tianjin Key Laboratory of Electronic Materials and Devices, School of Electronics and Information Engineering, Hebei University of Technology, 5340 Xiping Road, Tianjin 300401, P. R. China

† Electronic supplementary information (ESI) available. See DOI: <https://doi.org/10.1039/d2tc01395a>

CsPbBr₃, Cs₄PbBr₆ has a wider bandgap of 3.9 eV, which is attributed to its [PbBr₆]⁴⁻ octahedral structure completely isolated by Cs⁺ cations.^{32,34,35} During previous research, it is found that the ratio between CsPbBr₃ and Cs₄PbBr₆ in the film can be adjusted by controlling the molar ratio of CsBr/PbBr₂ in the precursor solution. As a result, a blue shift in the photoluminescence (PL) wavelength was observed as CsBr was increased in the Cs–Pb–Br film, induced *via* the strength of the confinement from incorporating Cs₄PbBr₆ into the CsPbBr₃ film.^{36–39} Moreover, the incorporated Cs–Pb–Br film exhibits an enhanced luminescence efficiency in the green region. This is attributed to the decreased surface trap states on CsPbBr₃, which is passivated by the formation of Cs₄PbBr₆. However, the effect of spatial confinement by Cs₄PbBr₆ is very limited, and the pure Cs–Pb–Br composite could not realize blue PeLEDs.^{40–47} Therefore, there is an urgent need to study the spatial confinement in the CsPbBr₃:Cs₄PbBr₆ system, and the feasibility of achieving blue PeLEDs.

Herein, we demonstrate a sky-blue PeLED based on the pure cesium lead bromide system for the first time. A NiO_x layer is used to control the perovskite phase component instead of the traditional poly(3,4-ethylenedioxythiophene)-poly(styrene sulfonate) (PEDOT:PSS) anodic interfacial layer. A blue shift is observed in the electroluminescence spectra (from 515 to 491 nm) by adjusting the Cs/Pb ratio in the precursor solution, and an optimized stable blue PeLED is achieved with a maximum luminance of 1610 cd m⁻² and a maximum EQE of 1.58%. Further analysis indicates that the NiO_x layer promoted the formation of Cs₄PbBr₆, which confined the crystal growth of CsPbBr₃. Compared with the traditional PEDOT:PSS interface, the spatial confinement effect in the CsPbBr₃:Cs₄PbBr₆ composition is strengthened by the NiO_x interface, and a sky-blue

PeLED was subsequently obtained. This study will open up a new avenue through interfacially induced phase regulation for developing blue PeLEDs.

Results and discussion

In this work, we prepared pure bromide-based blue PeLEDs with the structure of indium tin oxide (ITO)/NiO_x (10 nm)/perovskite (60 nm)/TPBi (30 nm)/LiF (1 nm)/Al (80 nm). Fig. 1a and b show the device structure schematic and cross-sectional scanning electron microscopy (SEM) image of the PeLED, where NiO_x serves as an anode interface layer instead of PEDOT:PSS to transport holes. NiO_x used here is synthesized according to the methods previously reported, which are described in the Experimental section. In this work, our synthesized NiO_x has three diffraction peaks, namely 37.1°, 43.2°, and 62.4°, which correspond to the (111), (200), and (220) planes, respectively, of NiO_x (PDF #47-1049), together with a particle size of less than 10 nm. In addition, it has a large bandgap and a deep valence band of -5.28 eV, which matches well with the energy level of different perovskites, especially blue-emitting perovskites (Fig. S1, ESI†).^{48,49} To investigate the effects of different Cs/Pb ratios on the NiO_x-based PeLEDs, we prepared PeLEDs using perovskite precursor solutions with different CsBr/PbBr₂ molar ratios of 1.4:1, 1.6:1, 1.8:1 and 2.0:1. Fig. 1c shows the normalized electroluminescence spectra (EL) of the PeLEDs based on the NiO_x hole-transport layer. Firstly, we found that as the Cs/Pb ratio was increased, the EL peak position exhibits a blueshift, from 515 nm at the Cs/Pb ratio of 1.4:1 to 491 nm at the Cs/Pb ratio of 1.8:1, which belongs to the sky-blue range. Then, as the Cs/Pb ratio was

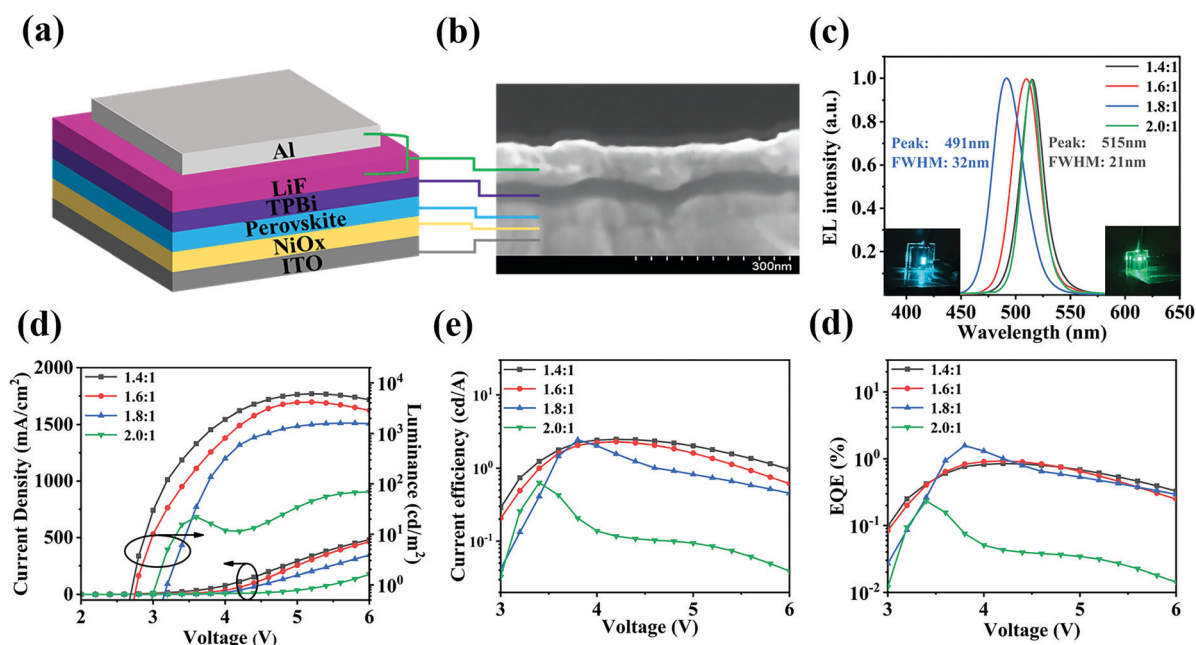


Fig. 1 (a) Schematic representation and (b) cross-sectional SEM image of the PeLED. (c) Normalized EL spectra, (d) J - V , (e) CE- V , and (f) EQE- V curves of PeLEDs with different CsBr:PbBr₂ molar ratios of 1.4:1, 1.6:1, 1.8:1, and 2.0:1.

increased further, the EL peak position returned to the green region (514 nm). It is clearly seen that a blue emission can be easily regulated by tuning the Cs/Pb ratio of the devices based on the NiO_x hole-transport layer. Moreover, at the same time, compared with the green PeLED, the full-width at half-maximum (FWHM) of the EL spectrum is broadened for the blue PeLED, suggesting the formation of different luminescence components. Fig. 1d–f shows the current density–voltage–luminance (*J–V–L*), current efficiency–voltage (*CE–V*) and EQE–voltage (*EQE–V*) curves for the above devices, and the device performance is summarized in Table 1. The normal green-emitting device with a Cs/Pb ratio of 1.4 : 1 shows poor EL characteristics due to the number of defect states at the grain boundaries. Under the same conditions, the realized blue-emitting PeLED with a Cs/Pb ratio of 1.8 : 1 displays a maximum luminance of 1610 cd m⁻², a maximum CE of 2.45 cd A⁻¹, and a maximum EQE of 1.58%. The EQE of this blue PeLED is nearly two times higher than that of the green PeLED, indicating a reduced defect density and enhanced radiative recombination efficiency. Although a blueshift is also found in the PeLEDs based on the PEDOT:PSS anode interface layer, the changes range from 517 to 510 nm, which is still within the green region (Fig. S2, ESI†). The PL spectra of perovskite films based on the NiO_x and PEDOT:PSS interfaces also exhibit a similar trend as the EL spectra (Fig. S3, ESI†), indicating that NiO_x plays a key role in the realization of blue PeLEDs.

To investigate the effect of the NiO_x interface layer on the blue PeLED, the crystallization properties of perovskite films grown on PEDOT:PSS and NiO_x were compared *via* their X-ray diffraction (XRD) spectra, as shown in Fig. 2a and b. It is found that perovskite films deposited on both PEDOT:PSS and NiO_x display significant diffraction peaks at $2\theta = 15.2^\circ, 21.5^\circ, 30.7^\circ,$ and 37.7° , which are indexed to the (100), (110), (200), and (211) lattice planes (PDF#18-0364), respectively, that belong to CsPbBr₃ crystals. At the same time, a series of diffraction peaks is also observed at $2\theta = 12.9^\circ, 22.4^\circ, 25.34^\circ, 39^\circ$ for the perovskite film deposited on NiO_x with the CsBr : PbBr₂ molar ratio of 1.8 : 1, which are identified as the (110), (300), (024), and (324) reflections, respectively, ascribed to the characteristic peaks of Cs₄PbBr₆ (PDF#73-2478). After this comparison, we speculated that the mixed phase of CsPbBr₃ and Cs₄PbBr₆ was formed in the perovskite film deposited on NiO_x, whereas in the perovskite film deposited on PEDOT:PSS there was mainly CsPbBr₃ and no obvious formation of Cs₄PbBr₆. This suggests that Cs₄PbBr₆ can only be formed in the perovskite film deposited on NiO_x with specific Cs/Pb proportions. Meanwhile, an exclusive absorption peak for Cs₄PbBr₆ at 315 nm was also

observed from the perovskite film (CsBr : PbBr₂ molar ratio of 1.8 : 1) deposited on NiO_x, which further confirmed the existence of Cs₄PbBr₆ (Fig. S4a, ESI†).³² The emergence of Cs₄PbBr₆ confined the growth of CsPbBr₃ grains, and electrons and holes formed in the NiO_x-based perovskite film, providing a favorable support for the spectral blueshift. To further analyze the effect of Cs₄PbBr₆ on the energy band, absorption and ultraviolet photoelectron spectra (UPS) of the perovskite films based on the different hole-transport layers were obtained, and the energy-band diagrams of the PeLED prepared based on PEDOT:PSS and NiO_x are shown in Fig. 2c and d, respectively. The energy-band levels of ITO, PEDOT:PSS, TPBi, and Al/LiF were obtained from the literature,^{50–52} and the energy levels for the perovskite films grown on PEDOT:PSS and NiO_x were determined *via* Tauc plots and UPS spectra (Fig. S4, ESI†).⁴⁸ Compared with the calculated bandgap of the PEDOT:PSS/perovskite (2.38 eV), a wider bandgap of 2.49 eV was achieved for the NiO_x/perovskite. As seen from the energy-band diagrams, NiO_x has a lower valence band of -5.28 eV than that of PEDOT:PSS (-5.04 eV),^{51,53} which is more favorable to match with the wide bandgap of the blue-emitting perovskite material. Meanwhile, the valence band of the perovskite film was significantly increased from -5.84 to -5.46 eV after introducing NiO_x instead of PEDOT:PSS, which is attributed to the formation of the CsPbBr₃ and Cs₄PbBr₆ composition.⁴⁵ The reduction of the valence band for the perovskite film based on NiO_x further facilitates hole injection for the blue PeLED.

To understand the effect of different Cs/Pb ratios on the morphology of the perovskite films, atomic force microscopy (AFM) and SEM images of the perovskite films deposited on NiO_x with different CsBr : PbBr₂ molar ratios were investigated, as shown in Fig. 3. The perovskite film with the CsBr : PbBr₂ molar ratio of 1.4 : 1 shows uniform granular crystals with a root-mean-square (RMS) of 8.8 nm, which corresponds to the green-emitting CsPbBr₃. As the Cs/Pb ratio is increased to 1.8, there emerge two completely different phases that include fine crystalline particles and large grains assembled in lamellar structures. We deduce that the lamellar structures belong to the Cs₄PbBr₆ crystals, which restricted the growth of granular grains to achieve small-sized CsPbBr₃, resulting in a smoother morphology with an RMS of 5.9 nm. As the Cs/Pb ratio is increased further to 2.0, the lamellar structures almost disappear again, which is attributed to the excess CsBr hindering the Cs₄PbBr₆ formation. Meanwhile, the morphology of the perovskite film based on PEDOT:PSS was also studied for comparison, in which there are no obvious lamellar Cs₄PbBr₆ crystals with a higher roughness (Fig. S5, ESI†). In addition, compared with the contact angle of the perovskite precursor solution on PEDOT:PSS (23.08°), the contact angle of the perovskite precursor solution on NiO_x has a smaller value of 15.54°, indicating that the perovskite precursor solution has better wettability on NiO_x (Fig. S6, ESI†). The relationship between the contact angle θ and the energy for crystal nucleation can be described using the following expression:⁵¹

$$\Delta G_{\text{heterogeneous}} = \Delta G_{\text{homogeneous}} \times f(\theta)$$

$$f(\theta) = \frac{1}{4}(1 - \cos\theta)^2(2 + \cos\theta)$$

Table 1 Summary of the EL properties of the PeLEDs under different conditions

Device CsBr : PbBr ₂	EL (nm)	FWHM (nm)	<i>L</i> (cd m ⁻²)	CE (cd A ⁻¹)	EQE (%)
1.4 : 1	515	24	6070	2.49	0.85
1.6 : 1	510	29	4170	2.31	0.94
1.8 : 1	491	32	1610	2.45	1.58
2.0 : 1	514	21	96	0.6	0.23

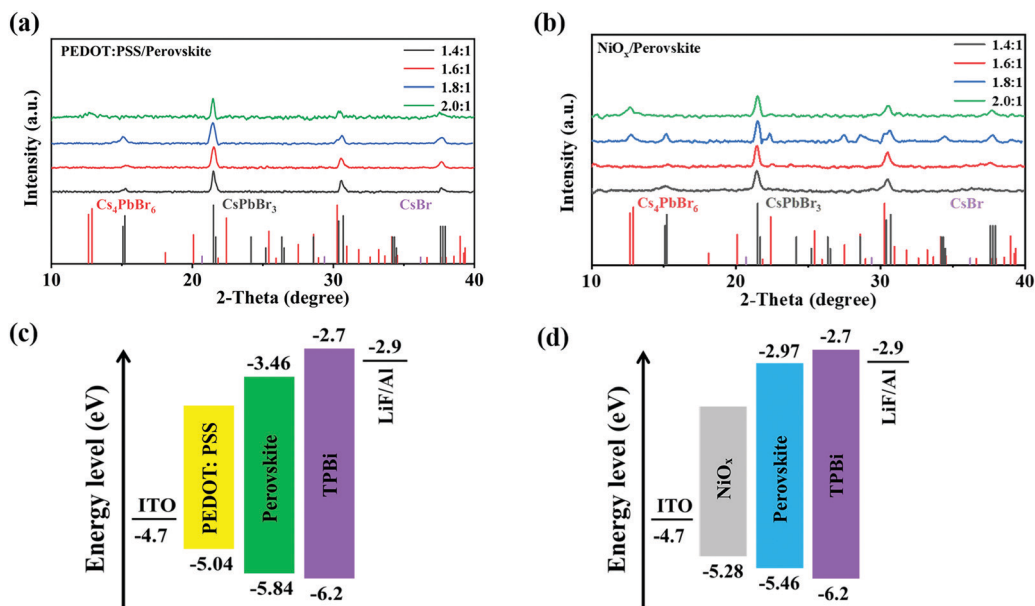


Fig. 2 XRD patterns of perovskite films with different CsBr : PbBr₂ molar ratios deposited on (a) PEDOT:PSS and (b) NiO_x, respectively. Energy-band diagrams of the PeLED prepared based on (c) PEDOT:PSS and (d) NiO_x, respectively.

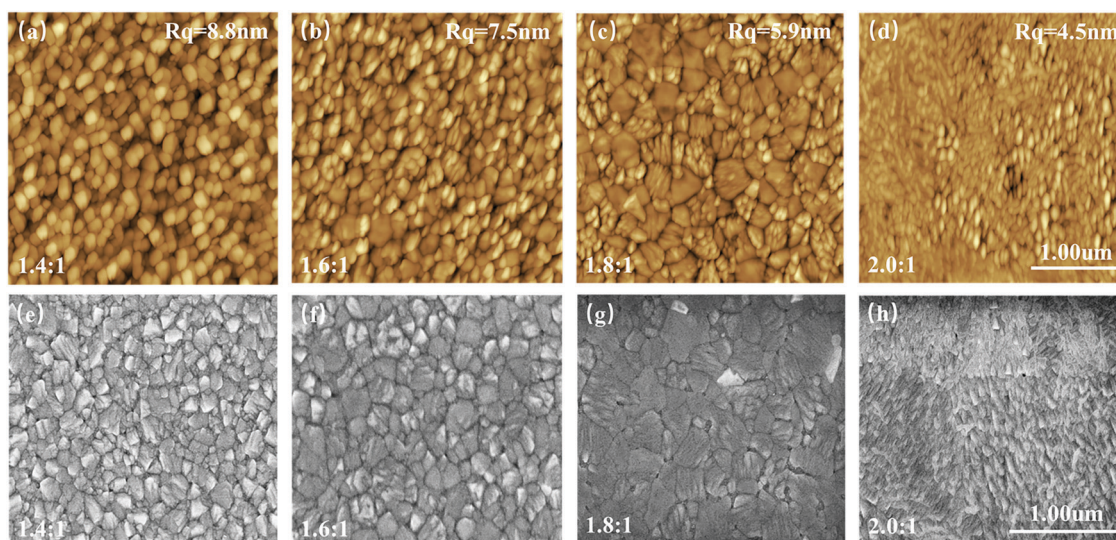


Fig. 3 (a–d) AFM, and (e–h) SEM images of perovskite films deposited on NiO_x with different CsBr : PbBr₂ molar ratios.

where $\Delta G_{\text{heterogenous}}$ and $\Delta G_{\text{homogenous}}$ represent the crystal nucleation energy of heterogeneous nucleation and homogeneous nucleation, respectively. It can be seen from the formula that the heterogeneous nucleation energy is proportional to the contact angle, that is, the larger the contact angle, the more nucleation energy is required and the more difficult the nucleation is. By contrast, the smaller the contact angle, the easier nucleation. Therefore, a smaller contact angle based on NiO_x would have a lower heterogeneous nucleation energy, which makes the nucleation easier, facilitating the formation of compact lamellar Cs₄PbBr₆.⁵⁴ Therefore, the above results clearly reveal that the NiO_x layer plays an important role in the formation of the CsPbBr₃ : Cs₄PbBr₆

composition in the perovskite film, which makes a major contribution to the blue PeLED.

To further investigate the interaction between NiO_x and the perovskite films, X-ray photoelectron spectroscopy (XPS) was carried out. Fig. 4a and b show the XPS spectra of Ni and O elements in NiO_x and NiO_x/perovskite, respectively. It was found that after deposition of the perovskite, the Ni 2p peaks represented by NiOOH, Ni₂O₃, and NiO move towards a lower binding energy (BE), and the O1s peaks corresponding to the –OH of NiOOH move towards a higher binding energy (BE), indicating a significant interaction between NiO_x and the perovskite.^{48,55–57} Herein, the shift in binding energy can be

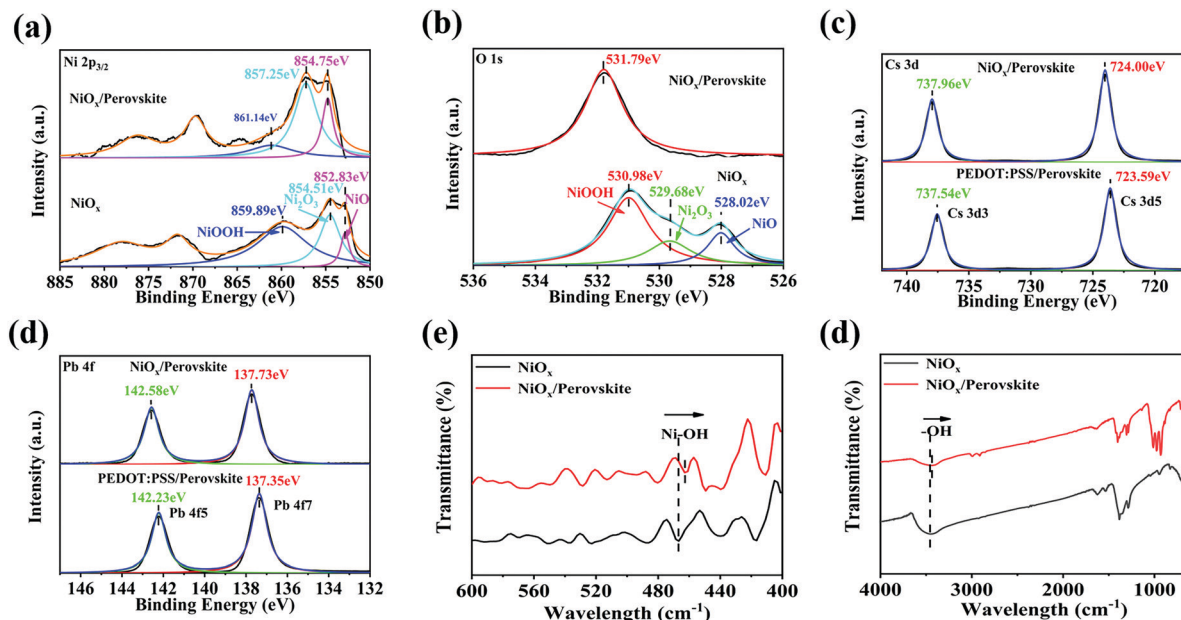


Fig. 4 XPS spectra of (a) Ni $2p_{3/2}$, and (b) O $1s$ for NiO_x and $\text{NiO}_x/\text{perovskite}$. XPS spectra of (c) Cs $3d$, and (d) Pb $4f$ based on NiO_x and PEDOT:PSS. (e and f) FTIR spectra for NiO_x and $\text{NiO}_x/\text{perovskite}$. The Cs/Pb ratio is 1.8.

attributed to coordination reactions between hydroxyl groups and lead, which would favor regulation of the crystallization of the perovskite films and the promotion of interfacial charge transfer, facilitating the formation of Cs_4PbBr_6 in the presence of moderate amounts of CsBr. To compare the effect of different hole-transport layers on the perovskite film, the characteristic peaks of Cs and Pb were also measured, as shown in Fig. 4c and d, respectively, from which the Cs/Pb atomic ratios in the perovskite films under different hole-transport layers could be calculated. The Cs/Pb atomic ratios of the perovskite films on NiO_x and PEDOT:PSS are 1.4 and 1.1, respectively. The higher Cs/Pb ratio in $\text{NiO}_x/\text{perovskite}$ illustrates that the NiO_x is more conducive to growth of the high-Cs ratio Cs_4PbBr_6 . To further explore the role of chemical bonding between NiO_x and the perovskite, Fourier transform infrared (FTIR) spectroscopy was studied using NiO_x and $\text{NiO}_x/\text{perovskite}$ powder samples, as seen in Fig. 4e and f. It was found that after deposition of the perovskite, the characteristic peaks of Ni–OH at 466.7 cm^{-1} and surface –OH at 3457 cm^{-1} all weakened and moved to 462 cm^{-1} and 3476 cm^{-1} , respectively, which further confirms that the –OH on the surface of NiO_x can interact with the perovskite, thus explaining in more detail the reason for the generation of Cs_4PbBr_6 .⁵⁸

To provide further insight into the relationship between the charge-recombination dynamics and the device performance, photoluminescence quantum yield (PLQY) measurements and time-resolved PL (TRPL) spectra of the perovskite films with different CsBr:PbBr₂ molar ratios based on the two anode interface layers were carried out (Fig. S7, ESI[†]), and details of these parameters are listed in Table S2 (ESI[†]). It can be seen that the perovskite films with a Cs/Pb ratio of 1.8 have the highest PLQY and the shortest average PL lifetime (τ) on both

PEDOT:PSS and NiO_x layers. Moreover, the average PL lifetimes of perovskite films with different Cs/Pb ratios show the same change trend on both PEDOT:PSS and NiO_x layers. According to the relationship between the non-radiative recombination rate k_{nr} and the radiative recombination rate k_r :⁵¹

$$\text{PLQY} = \frac{k_r}{k_r + k_{\text{nr}}}$$

$$\tau = \frac{1}{k_r + k_{\text{nr}}}$$

the non-radiative decay rate k_{nr} and the radiative decay rate k_r can be expressed as:

$$k_{\text{nr}} = \frac{1 - \text{PLQY}}{\tau}$$

$$k_r = \frac{\text{PLQY}}{\tau}$$

Therefore, the perovskite films with the Cs/Pb ratio of 1.8 have the highest radiative decay rate, which is consistent with the best device performance at this ratio in both the PEDOT:PSS- and NiO_x -based devices. However, due to the lower PL lifetime in the blue-emission range, the non-radiative decay rate of the perovskite film deposited on NiO_x with the Cs/Pb ratio of 1.8 shows a high value of $5.9 \times 10^8\text{ s}^{-1}$. To further investigate the defect density of the NiO_x -based perovskite films, hole-only devices with the structure of ITO/ $\text{NiO}_x/\text{perovskite}/\text{MoO}_3/\text{Al}$ were prepared and the trap density was calculated using the following equation:⁵⁰

$$N_{\text{defects}} = \frac{2\varepsilon_0\varepsilon_r V_{\text{TFL}}}{qL^2}$$

Table 2 Summary of the performance parameters for the blue PeLEDs

Emitting layer	EL (nm)	L (cd m ⁻²)	EQE (%)	T_{50} (min)	FWHM (nm)
CsPbBr ₃ QD ⁸	479	NA	12.3	20 min@100 cd m ⁻²	20
PEA ₂ (Rb _x Cs _{1-x}) ₂ Pb ₃ Br ₁₀ ⁶⁰	475	100.6	1.35	14.5 min@15 cd m ⁻²	20
Rb _{0.13} Cs _{0.87} PbBr _{2.22} Cl _{0.78} ³¹	484	9243	1.66	—	16
CsPbBr ₃ + PEABr ³³	484	45	0.13	3.5 min@4V	34
PEA ₂ NPA ₁ Cs ₂ Pb ₃ Br ₁₂ ⁶¹	485	1200	2.62	8.8 min@15 cd m ⁻²	23
CsPbBr ₃ + PBABr ⁶²	487	643.8	4.34	3.87 min@12 cd m ⁻²	29
CsPbBr ₃ NPLs ⁶³	469	19.2	1.42	0.7 min@1 mA cm ⁻²	25
This work	491	1610	1.58	8.5 min@100 cd m ⁻²	32

where ϵ_0 and ϵ_r are the vacuum permittivity and relative permittivity, respectively, q is the elementary charge, L is the thickness of the perovskite film, and V_{TFL} is the onset voltage of the trap-filled confinement region (Fig. S8 and Table S3, ESI†). The trap density decreases as the Cs/Pb ratio is increased, and reaches the lowest value when Cs₄PbBr₆ appears under the Cs/Pb ratio of 1.8. However, as the Cs/Pb ratio is increased further to 2.0, the hole current density shows a sharp decrease.⁵⁹ The extremely unbalanced carrier injection at this ratio results in the poor PeLED performance as seen in Fig. 1. Anyway, the luminescence kinetics of perovskite films based on the NiO_x interface layer should be further studied in the future.

Finally, we summarize the performance parameters of blue PeLEDs based on the CsPbBr₃ system in Table 2. The blue PeLED prepared in this work exhibits stable EL spectra under different voltages and has a lifetime of $T_{50} = 8.5$ min at the luminescence peak of 491 nm and an initial luminance of 100 cd m⁻² (Fig. S9, ESI†). It is worth mentioning that among the reported blue PeLEDs based on CsPbBr₃, our blue PeLED does not use any elemental doping and has the simplest preparation process.

Conclusions

In summary, a blue PeLED based on a pure bromide system without any doping using a NiO_x hole-transport layer has been prepared for the first time. Compared with the traditional hole-transport layer of PEDOT:PSS, the NiO_x layer has rich -OH groups on its surface, which are more favorable for interaction with the perovskite and the formation of Cs₄PbBr₆, which restricts the growth of CsPbBr₃ and subsequently leads to the blue-emitting perovskite film. The all-inorganic CsPbBr₃:Cs₄PbBr₆ PeLED has high thermal and spectral stability, and the prepared blue device has a maximum luminance of 1610 cd m⁻², a maximum EQE of 1.58%, and an EL wavelength of 491 nm. This work will open up a new avenue for the study of blue PeLEDs with interfacially controlled phase contents. Although this work is innovative, it still has certain limitations. The prepared perovskite light-emitting diodes have a low color purity, and their efficiency and brightness still need to be improved. In future work, we will continue to study PeLEDs based on the NiO_x anode interface layer, to deeply understand the dynamic process of blue-light emission and the defect-formation mechanism, and conduct further research for the development of efficient and stable blue-light PeLEDs.

Experimental materials

TPBI was purchased from Xi'an Polymer Light Technology Company, CsBr was purchased from Kanto Chemical Company, PbBr₂ was purchased from Liaoning Preferred New Energy Technology Company, nickel nitrate hexahydrate (Ni(NO₃)₂·6H₂O) and sodium hydroxide (NaOH) were purchased from Inokai Technology Co.

Preparation of NiO_x nanoparticles

29 g of Ni(NO₃)₂·6H₂O was weighed and 20 mL of deionized water was added and stirred to dissolve to obtain a dark-green solution; an aqueous NaOH solution with a mass concentration of 400 mg mL⁻¹ was prepared and the NaOH solution was added dropwise to the dark-green solution, and then the pH value of the Ni(NO₃)₂·6H₂O aqueous solution was adjusted close to 10. After stirring for 30 min, the suspension was filtered under a vacuum. After vacuum filtration, the green mucilage was washed three times with deionized water and ethanol, respectively, to remove soluble impurities. Then, the glue was transferred to a vacuum oven at 80 °C overnight to obtain a green powder. The green powder was ground, ultrasonically shaken for 10 min, then moved to a muffle furnace and calcined at 270 °C for 2 h, paying attention to the heating rate, to obtain deep black NiO_x nanoparticles. The prepared NiO_x nanoparticles were dispersed in deionized water at a set concentration.

Preparation of perovskite precursor solutions

The concentration of the perovskite precursor solution was kept constant at 170 mg mL⁻¹, and the molar ratio of CsBr:PbBr₂ in the solution was 1.4:1, 1.6:1, 1.8:1, and 2.0:1, respectively. The DMSO solution was added to a mixture of CsBr and PbBr₂ powder samples in a glove box and stirred at 45 °C until a clear and transparent chalcogenide precursor solution was obtained. Before device preparation, the glass/ITO substrates were cleaned with acetone, ethanol, and deionized water in sequence and then dried, followed by UV-O₃ treatment of the substrates for 30 min.

Preparation and characterization of perovskite films and PeLEDs

The NiO_x aqueous dispersion of 15 mg mL⁻¹ and PEDOT:PSS solution were deposited onto the glass/ITO substrate *via* one-step spin-coating at 2500 rpm for 1 min, followed by UV-O₃

treatment of the NiO_x film for 10 min. Then, the substrates were transferred to a glove box filled with nitrogen, and the perovskite films were deposited *via* spin-coating at 4500 rpm for 60 s and heated at 70 °C for 10 min. Finally, TPBI (30 nm), LiF (1 nm), and Al (80 nm) were sequentially deposited using a vacuum coater under a vacuum of less than 4×10^{-4} Pa. In this experiment, SEM (Hitachi S4800) and AFM (Shimadzu SPA-9700) were used to characterize the surface morphology of the NiO_x, PEDOT:PSS, and perovskite emission layers. XRD spectra of the PeLEDs were collected using a powder diffraction device (Bruker Advance D8-ray). The absorption spectra of the perovskite layers were measured using an ultraviolet-visible spectrophotometer (Shimadzu UV-3101PC). Steady-state PL spectra of the perovskite layers were measured using a Hitachi F-7000 fluorescence spectrometer. XPS and UPS were measured using a Thermo Scientific NEXSA instrument. The current density–voltage curves and luminance–voltage curves of the device were measured using a Keithley 2611 digital source meter and a luminance meter (Konica-Minolta LS-110). PLQY and TRPL tests were carried out using an FLS920 steady-state/transient fluorescence spectrometer.

Conflicts of interest

There are no conflicts to declare.

Acknowledgements

This work is supported by the National Science Foundation of China (No. 62175235, 61875195, 51973208, 61975256 and 62035013), the Jilin Province Science and Technology Research Project (No. 20200401074GX), and the Project supported by the Dawn Talent Training Program of CIOMP.

Notes and references

- Z. Tan, R. Moghaddam, M. Lai, P. Docampo, R. Higler, F. Deschler, M. Price, A. Sadhanala, L. Pazos and D. Credgington, *Nat. Nanotechnol.*, 2014, **9**, 687–692.
- C. H. Kang, I. Dursun, G. Liu, L. Sinatra, X. Sun, M. Kong, J. Pan, P. Maity, E.-N. Ooi and T. K. Ng, *Light: Sci. Appl.*, 2019, **8**, 1–12.
- Y. Miao, L. Cheng, W. Zou, L. Gu, J. Zhang, Q. Guo, Q. Peng, M. Xu, Y. He and S. Zhang, *Light: Sci. Appl.*, 2020, **9**, 1–6.
- Y. H. Kim, S. Kim, A. Kakekhani, J. Park and T. W. Lee, *Nat. Photonics*, 2021, **15**, 1–8.
- Z. Chu, Q. Ye, Y. Zhao, F. Ma, Z. Yin, X. Zhang and J. You, *Adv. Mater.*, 2021, **33**, 2007169.
- Y. Hassan, J. H. Park, M. L. Crawford, A. Sadhanala and H. J. Snaith, *Nature*, 2021, **591**, 72–77.
- C. Yu, N. Wang, T. He, J. Guo, Y. Wei, C. Hong, Y. Miao, Z. Wei, P. Kang and Y. He, *Nature*, 2018, **562**, 249–253.
- Y. Dong, Y.-K. Wang, F. Yuan, A. Johnston, Y. Liu, D. Ma, M.-J. Choi, B. Chen, M. Chekini and S.-W. Baek, *Nat. Nanotechnol.*, 2020, **15**, 668–674.
- M. Karlsson, Z. Yi, S. Reichert, X. Luo, W. Lin, Z. Zhang, C. Bao, R. Zhang, S. Bai and G. Zheng, *Nat. Commun.*, 2021, **12**, 1–10.
- Y. Liu, Z. Li, J. Xu, Y. Dong, B. Chen, S. M. Park, D. Ma, S. Lee, J. E. Huang and S. Teale, *J. Am. Chem. Soc.*, 2022, **144**, 4009–4016.
- N. K. Kumawat, X. K. Liu, D. Kabra and F. Gao, *Nanoscale*, 2019, **11**, 2109–2120.
- S. Hou, M. K. Gangishetty, Q. Quan and D. N. Congreve, *Joule*, 2018, **2**, 2421–2433.
- J. Xing, Y. Zhao, M. Askerka, L. N. Quan, X. Gong, W. Zhao, J. Zhao, H. Tan, G. Long and L. Gao, *Nat. Commun.*, 2018, **9**, 1–8.
- Z. Li, Z. Chen, Y. Yang, Q. Xue, H.-L. Yip and Y. Cao, *Nat. Commun.*, 2019, **10**, 1–10.
- H. Wang, X. Zhao, B. Zhang and Z. Xie, *J. Mater. Chem. C*, 2019, **7**, 5596–5603.
- S. Peng, S. Wang, D. Zhao, X. Li and Z. Tang, *Small Methods*, 2019, **3**, 1900196.
- Z. Chu, Y. Zhao, F. Ma, C. X. Zhang and J. You, *Nat. Commun.*, 2020, **11**, 1–8.
- Z. Ren, L. Li, J. Yu, R. Ma and W. Choy, *ACS Energy Lett.*, 2020, **5**, 2569–2579.
- Y. Zou, H. Xu, S. Li, T. Song and B. Sun, *ACS Photonics*, 2019, **6**, 1728–1735.
- Z. Ren, X. Xiao, R. Ma, H. Lin and W. Choy, *Adv. Funct. Mater.*, 2019, **29**, 1905339.
- M. Wor, Ku, Q. He, L. J. Xu, J. Hong and B. Ma, *ACS Appl. Mater. Interfaces*, 2020, **12**, 45056–45063.
- F. Zhang, B. Cai, J. Song, B. Han and H. Zeng, *Adv. Funct. Mater.*, 2020, **30**, 2001732.
- S. Zeng, S. Shi, S. Wang and Y. Xiao, *J. Mater. Chem. C*, 2020, **8**, 1319–1325.
- X. K. Liu, W. Xu, S. Bai, Y. Jin and F. Gao, *Nat. Mater.*, 2020, **20**, 10–21.
- Z. Xiao, R. A. Kerner, L. Zhao, N. L. Tran, K. M. Lee, T. W. Koh, G. D. Scholes and B. P. Rand, *Nat. Photonics*, 2017, **11**, 108–115.
- H. Huang, A. S. Sussha, S. V. Kershaw, T. F. Hung and A. L. Rogach, *Adv. Sci.*, 2015, **2**, 1500194.
- F. Zhang, D. H. Kim, H. Lu, J. S. Park, B. Larson, J. Hu, L. Gao, C. Xiao, O. Reid and X. Chen, *J. Am. Chem. Soc.*, 2019, **141**, 5972–5979.
- T. Wu, J. Li, Y. Zou, H. Xu and B. Sun, *Angew. Chem.*, 2019, **132**, 4099–4105.
- P. Todorović, D. Ma, B. Chen, R. Quintero-Bermudez, M. I. Saidaminov, Y. Dong, Z. H. Lu and E. H. Sargent, *Adv. Opt. Mater.*, 2019, **7**, 1901440.
- S. Hou, M. K. Gangishetty, Q. Quan and D. N. Congreve, *Joule*, 2018, **2**, 2421–2433.
- H. Wang, Y. Xu, J. Wu, L. Chen and Z. Xie, *J. Phys. Chem. Lett.*, 2020, **11**, 1411–1418.
- L. Song, L. Huang, Y. Liu, Y. Hu, X. Guo, Y. Chang, C. Geng, S. Xu, Z. Zhang and Y. Zhang, *ACS Appl. Mater. Interfaces*, 2021, **13**, 33199–33208.
- Y. Zou, H. Xu, S. Li, T. Song, L. Kuai, S. Bai, F. Gao and B. Sun, *ACS Photonics*, 2019, **6**, 1728–1735.

- 34 B. Kang and K. Biswas, *J. Phys. Chem. Lett.*, 2018, **9**, 830–836.
- 35 L. Wang, H. Liu, Y. Zhang and O. F. Mohammed, *ACS Energy Lett.*, 2019, **5**, 87–99.
- 36 Y. Shang, G. Li, W. Liu and Z. Ning, *Adv. Funct. Mater.*, 2018, **28**, 1801193.
- 37 Y. Ling, L. Tan, X. Wang, Y. Zhou, Y. Xin, B. Ma, K. Hanson and H. Gao, *J. Phys. Chem. Lett.*, 2017, **8**, 3266–3271.
- 38 J. Xu, W. Huang, P. Li, D. R. Onken, C. Dun, Y. Guo, K. B. Ucer, C. Lu, H. Wang and S. M. Geyer, *Adv. Mater.*, 2017, **29**, 1703703.
- 39 L. N. Quan, R. Quintero-Bermudez, O. Voznyy, G. Walters, A. Jain, J. Z. Fan, X. Zheng, Z. Yang and E. H. Sargent, *Adv. Mater.*, 2017, **29**, 1605945.
- 40 Y. Zhao, J. Wei, H. Li, Y. Yan, W. Zhou, D. Yu and Q. Zhao, *Nat. Commun.*, 2016, **7**, 10228.
- 41 L. Song, X. Guo, Y. Hu, Y. Lv, J. Lin, Z. Liu, Y. Fan and X. Liu, *J. Phys. Chem. Lett.*, 2017, 4148.
- 42 J. Li, X. Shan, S. Bade, T. Geske, Q. Jiang, X. Yang and Z. Yu, *J. Phys. Chem. Lett.*, 2016, 4059–4066.
- 43 Y. Ling, Y. Tian, X. Wang, J. C. Wang, J. M. Knox, F. Perez-Orive, Y. Du, L. Tan, K. Hanson and B. Ma, *Adv. Mater.*, 2016, **28**, 8983–8989.
- 44 M. K. Gangishetty, S. Hou, Q. Quan and D. N. Congreve, *Adv. Mater.*, 2018, **30**, 1706226.
- 45 P. Du, J. Li, L. Wang, L. Sun, X. Wang, X. Xu, L. Yang, J. Pang, W. Liang and J. Luo, *Nat. Commun.*, 2021, **12**, 1–10.
- 46 H. Cho, C. Wolf, J. S. Kim, H. J. Yun, J. S. Bae, H. Kim, J. M. Heo, S. Ahn and T. W. Lee, *Adv. Mater.*, 2017, **29**, 1700579.
- 47 H. Lin, L. Zhu, H. Huang, C. J. Reckmeier, C. Liang, A. L. Rogach and W. C. Choy, *Nanoscale*, 2016, **8**, 19846–19852.
- 48 F. Jiang, W. Choy, X. Li, D. Zhang and J. Cheng, *Adv. Mater.*, 2015, **27**, 2930–2937.
- 49 L. Liu, Z. Wang, W. Sun, J. Zhang, S. Hu, T. Hayat, A. Alsaedi and Z. A. Tan, *Chem. Commun.*, 2018, **54**, 13283–13286.
- 50 J. Ou, X. Guo, Y. Lv, Y. Fan, Y. Li, D. Zou, Z. Bao, L. Song and X. Liu, *ACS Appl. Mater. Interfaces*, 2021, **13**, 60571–60580.
- 51 J. Ou, X. Guo, L. Song, J. Lin, Y. Lv, Y. Fan, Y. Li, D. Zou, Z. Bao and X. Liu, *J. Mater. Chem. C*, 2021, **9**, 1025–1033.
- 52 H. Wang, Y. Xu, L. Chen, J. Wu, Q. Wang, B. Zhang and Z. Xie, *Org. Electron.*, 2021, **98**, 106299.
- 53 F. Wang, Z. Wang, X. Zhu, Y. Bai, Y. Yang, S. Hu, Y. Liu, B. You, J. Wang and Y. Li, *Small*, 2021, **17**, 2007363.
- 54 J. Wang, N. Wang, Y. Jin, J. Si, Z. K. Tan, H. Du, L. Cheng, X. Dai, S. Bai and H. He, *Adv. Mater.*, 2015, **27**, 2311–2316.
- 55 Y. Bai, H. Chen, S. Xiao, Q. Xue, T. Zhang, Z. Zhu, Q. Li, C. Hu, Y. Yang and Z. Hu, *Adv. Funct. Mater.*, 2016, **26**, 2950–2958.
- 56 H. Zhang, J. Cheng, F. Lin, H. He, J. Mao, K. S. Wong, A. K.-Y. Jen and W. C. Choy, *ACS Nano*, 2016, **10**, 1503–1511.
- 57 Z. Wang, Z. Luo, C. Zhao, Q. Guo, Y. Wang, F. Wang, X. Bian, A. Alsaedi, T. Hayat and Z. A. Tan, *J. Phys. Chem. C*, 2017, **121**, 28132–28138.
- 58 Y. Wang, H. Ju, T. Mahmoudi, C. Liu and Y. Mai, *Nano Energy*, 2021, **88**, 106285.
- 59 S. B. Naghadeh, B. Luo, Y.-C. Pu, Z. Schwartz, W. R. Hollingsworth, S. A. Lindley, A. S. Brewer, A. L. Ayzner and J. Z. Zhang, *J. Phys. Chem. C*, 2019, **123**, 4610–4619.
- 60 Y. Jiang, C. Qin, M. Cui, T. He, K. Liu, Y. Huang, M. Luo, L. Zhang, H. Xu and S. Li, *Nat. Commun.*, 2019, **10**, 1–9.
- 61 Y. Jin, Z. K. Wang, S. Yuan, Q. Wang, C. Qin, K. L. Wang, C. Dong, M. Li, Y. Liu and L. S. Liao, *Adv. Funct. Mater.*, 2020, **30**, 1908339.
- 62 N. Yantara, N. F. Jamaludin, B. Febriansyah, D. Giovanni, A. Bruno, C. Soci, T. C. Sum, S. Mhaisalkar and N. Mathews, *ACS Energy Lett.*, 2020, **5**, 1593–1600.
- 63 C. Zhang, Q. Wan, B. Wang, W. Zheng, M. Liu, Q. Zhang, L. Kong and L. Li, *J. Phys. Chem. C*, 2019, **123**, 26161–26169.